DAMIANO ZITO
CEO PROGOLD S.P.A. - TRISSINO VI - IT

Damiano Zito is the CEO for Progold S.p.A. in Trissino, Italy. He is a board member of Italian Jewellery Association as delegate for Norms and Innovation. He has 25 years of experience in the field. He is a recipient of the Santa Fé Symposium Ambassador Award and his company's R&D Department is a two-time winner of the Research Award.

In 2013 we studied and improved the quality level of the parts of jewelry pieces. Our effort was aimed at obtaining jewelry pieces through selective laser melting (SLM) with a quality level similar to investment cast pieces. This development work enabled us to obtain higher accuracy levels for gold alloys. This aim was reached with the use of parallel laser scanning, with a double laser scan and with the selection of optimum laser scanning parameters to avoid the well-known formation of surface-swelling defects. The addition of gallium was shown to increase the formation of this defect as well.
Moreover, in this experimentation we evaluated the effect of the structure of the support system of the pieces, namely shape, density and slope angle of piece walls. We used the optimum work parameters selected in preceding experiments and studied the effect of some elements favoring the absorption of laser radiation (Ge, Si, Pt). Thus, surface swelling, ejection of metal particles and surface roughness of the pieces were reduced.

Optimization of SLM Technology Main Parameters in the Production of Gold and Platinum Jewelry

DAMIANO ZITO
CEO PROGOLD S.P.A. - TRISSINO VI - IT

INTRODUCTION

In 2013 we studied and improved the quality level of the parts of jewelry pieces. Our effort was aimed at obtaining jewelry pieces through selective laser melting (SLM) with a quality level similar to investment cast pieces. This development work enabled us to obtain higher accuracy levels for gold alloys. This aim was reached with the use of parallel laser scanning, with a double laser scan and with the selection of optimum laser scanning parameters to avoid the well-known formation of surface-swelling defects. The addition of gallium was shown to increase the formation of this defect as well.

Moreover, in this experimentation we evaluated the effect of the structure of the support system of the pieces, namely shape, density and slope angle of piece walls. We used the optimum work parameters selected in preceding experiments and studied the effect of some elements favoring the absorption of laser radiation (Ge, Si, Pt). Thus, surface swelling, ejection of metal particles and surface roughness of the pieces were reduced.

EXPERIMENTAL PRACTICE

The experimental pieces were produced with a Realizer SLM™ 50 machine equipped with a 100W fiber laser having a 10mm spot and with a circular 70mm diameter build platform, placed in a chamber under an argon protective atmosphere. The alloy powders were produced with a gas atomizer, working in an environment fully protected with argon at atmospheric pressure. This atomizer guarantees the production of dry powder with a prevalence of spherical particles. Particle shape and absorbed humidity have an important effect on powder flowability when subjected to the action of the (screed) blade distributing the powder on the build platform. The evaluation of powder flowability was carried out with a Hall Flowmeter Funnel (ASTM B 213-03) and with a Carney Flowmeter Funnel (ASTM B 417-89). Apparent density was measured with a standard volume cup (ASTM B 212, B 329 and B 417).

Two powders were used for this study: a 750‰ red-gold alloy (alloy 1) and a 950‰ platinum alloy (alloy 2). Powder shape (Figures 1 and 2) and particle size distribution (Figures 3 and 4) were determined by SEM-EDS (Scanning Electron Microscope) observation and with a Malvern Laser Granulometer Hydro 2000S. The size of powder particles ranged from a few micrometers to about fifty micrometers. This result was obtained with a Giuliani sieve with 53 micrometers square mesh. The smallest particles were left in the powder, even though they appreciably reduced the flowability under the (screed) wiper of the build platform. The small particles were included because previous studies showed that they facilitate higher density and consequently lower porosity in production pieces.[1,2,3]

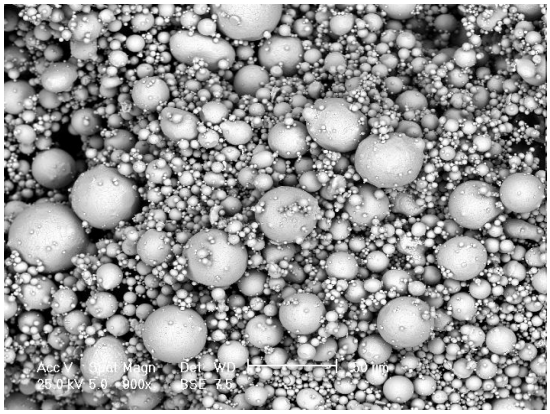

Figure 1 *750‰ gold alloy powder*

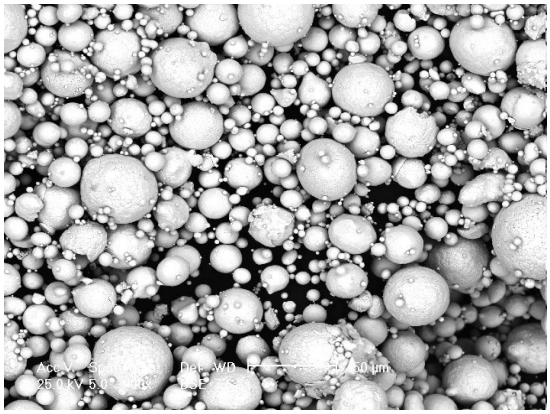

Figure 2 *950‰ platinum alloy powder*

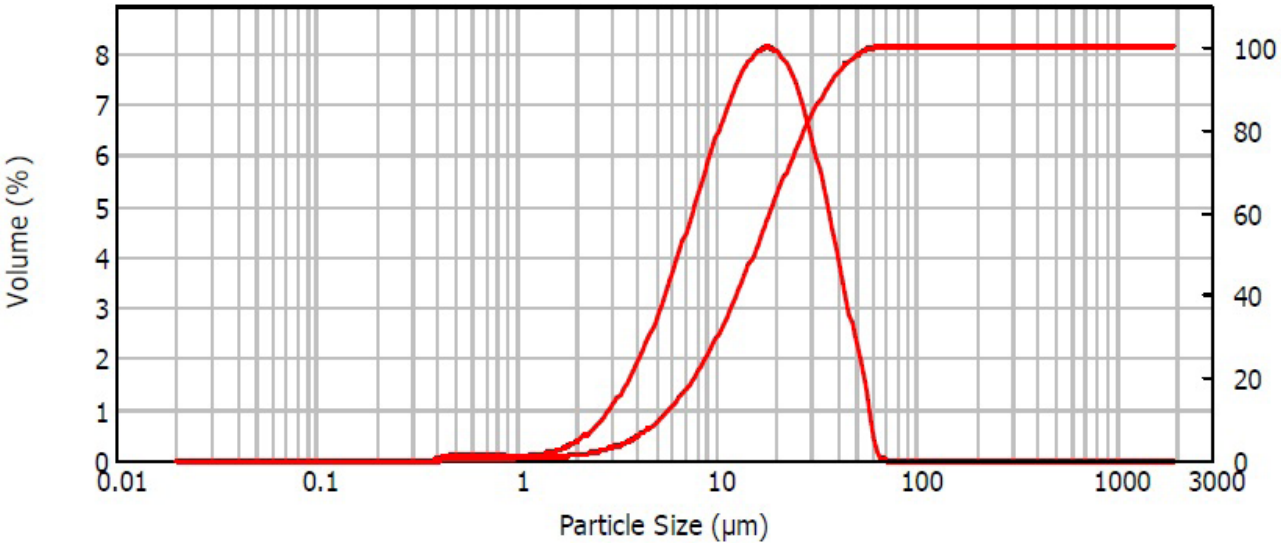

Figure 3 *Particle size distribution in the 750‰ gold alloy powder*

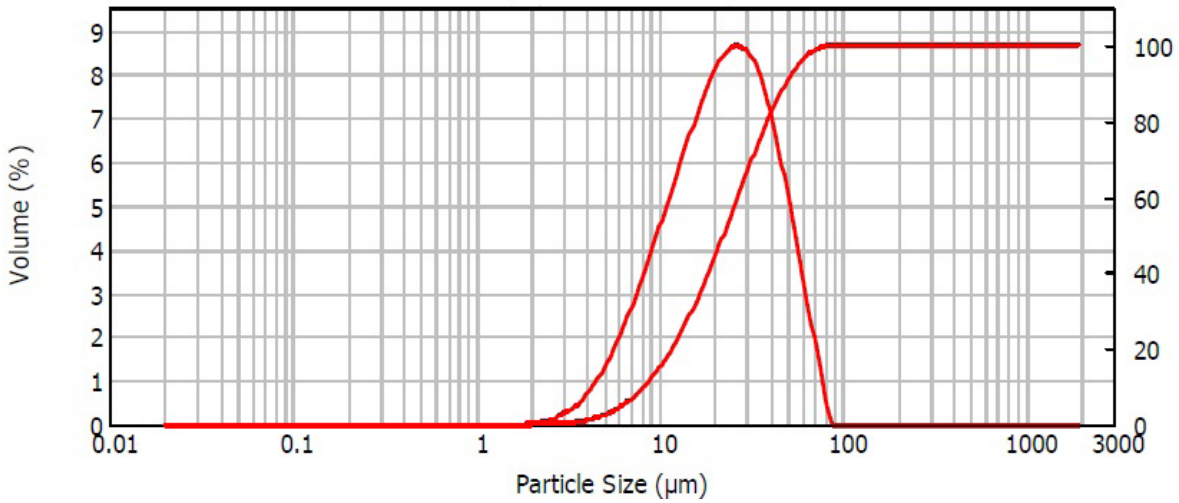

Figure 4 *Particle size distribution in the 950‰ platinum alloy powder*

Table 1 *Flowability, particle size range and apparent density as a function of particle size distribution*

ALLOY	Powder particle size range (µm)	d_{50} (µm)	d_{90} (µm)	Flowability Hall Flowmeter (s/50 g)	Flowability Carney Flowmeter (s/50 g)	Apparent density (g/cm^3)
1	0-53	15.44	35.90	No flow	5.5	8.70 ± 0.05
2	0-53	22.37	48.90	15.0	2.5	11.5 ± 0.05

d_{50} = maximum particle diameter in 50% of the powder volume
d_{90} = maximum particle diameter in 90% of the powder volume

Flowability tests showed that internal friction in the gold alloy powder was higher than in the platinum powder. This characteristic can be principally linked to the particle size distribution of the gold powder, where there is a higher fraction of small particles that hinder powder flowability. The chemical composition of the gold alloy was modified by the addition of elements selected to increase the absorption of laser radiation, thus reducing radiation reflection and diffusion by the powder particles that hinder melting of the powder.

Absorption of laser radiation by a metal (equation 1) is proportional to the square root of electrical resistivity.[4] Therefore, we looked for suitable elements to add that would increase electrical resistivity appreciably without compromising color and the mechanical characteristics required for jewelry alloys. Low boiling-point elements, like zinc, were avoided to reduce gas porosity caused by vapor formation in the molten alloy.

$$A = k\sqrt{x_r} \qquad \text{(equation 1)}$$

where:
A = absorptivity
k = a constant $(\Omega \cdot m)^{-1/2}$
ξ = electrical resistivity (Ω·m)

Evaluation of the surface of the raw product was carried out with a stereoscopic optical microscope, a metallographic microscope and a scanning electron microscope (SEM). Surface roughness in the build directions was measured with a Taylor Hobson$^{\text{Ò}}$ profilometer (Form Talysurf Intra2) equipped with a 2.0mm radius diamond-tipped carbon fiber feeler pin. Internal porosity was measured on the metallographic sections using Image J 1.48 B software.

In order to optimize laser parameters, for each of the alloy compositions we initially built the characteristic lamellar solids as reported in the previous papers.[2,5] This experimental solid had a parallelepiped shape with 10.0mm length, 5.0mm width and 5.0mm thickness. The minimal constant spacing between the different lamellae (named vectors) was 500mm (Figures 5 and 6). Examination of the single vectors of the experimental solids showed that lower laser parameters were required for the platinum than for the gold alloy to obtain a similar quality level (Table 2).

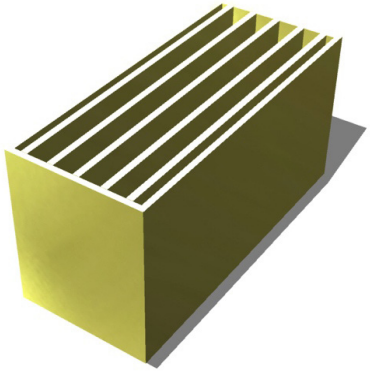

Figure 5 *Parallelepiped model produced with Magics 17.02 (Materialise)*

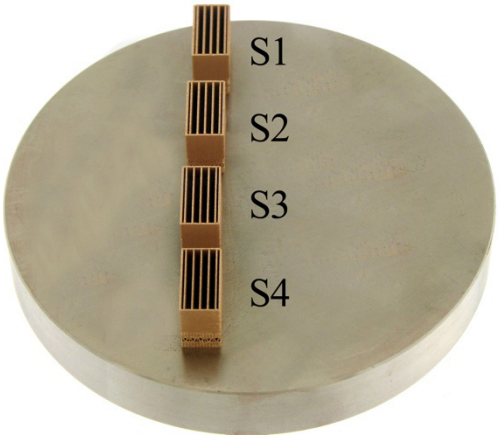

Figure 6 *Set of parallelepipeds in 750‰ gold alloy*

Table 2 *List of laser parameters used in the first set of pilot prototyping*

Test Name	Laser Power (W)	Exposure (µs)	Distance between spots on the contour (µm)	Distance between spots on the vectors (µm)	Scanning speed on the contour (m/s)	Scanning speed on the vectors (m/s)
S1	92.5	120	30	40	0.25	0.33
S2	82.5	120	30	40	0.25	0.33
S3	72.5	120	30	40	0.25	0.33
S4	62.5	120	30	40	0.25	0.33

Subsequently, a solid piece was built implementing the best laser parameters selected from the lamellar builds in each of the two alloys. This was done to see if the quality level required for jewelry pieces could be achieved. The software Magics 17.02 (Materialise) was used for the development of the supports for the experimental pieces. The shape of the specimens was modeled using Rhinoceros® 4.0 (McNeel) to be quite simple in order to reliably detect any dimensional changes caused by the building process.

The experimental pieces were parallelepipeds (bricks) with the following nominal dimensions: length 10.0mm, width 4.50mm and thickness 3.00mm (Figure 7). Actually, the finished thickness of the pieces was to be 2.80mm, but it was intentionally oversized to 3.0mm to accommodate subsequent grinding and polishing for the quality level evaluation. An oversize of 0.20mm was necessary to eliminate the spongy layer that is usually present at the base of items built by SLM and to avoid defects caused by support detachment. The usual production practice is to repair small defects deeper than 0.20mm or reject the piece if the defect is too awful.

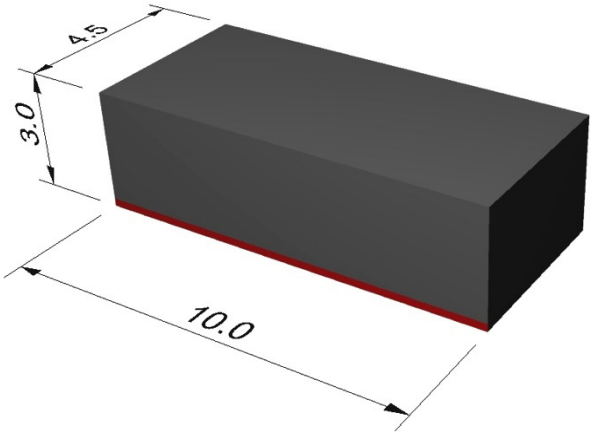

Figure 7 *Nominal dimensions and final thickness of the experimental pieces (bricks)*

After the bricks were removed from the build platform, they were embedded in epoxy resin (VariDur® 200, Buehler) with two adjacent surfaces exposed (Figures 8 and 9). This configuration allowed precise thickness measurements during grinding and polishing using optical microscopy. The longitudinal surface (A) was used to measure the thickness of the pieces so grinding and polishing could be stopped at the exact projected value and was also used to evaluate the depth of defects formed in the growth direction of the pieces. The thickness of the as-grown brick at the interface where the supports stopped and the surface of the bricks started was 3.00mm. Removing 0.20mm by grinding and polishing the transverse surface (B) removed a significant amount of normal defects and allowed quality evaluation on a surface equivalent to that of a finished piece of jewelry.

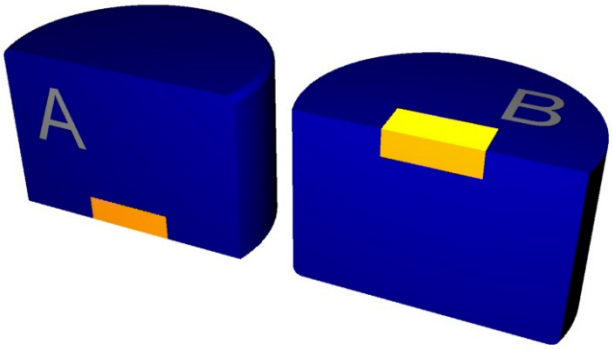

Figure 8 *Longitudinal (A) and transverse (B) surfaces for defect evaluation*

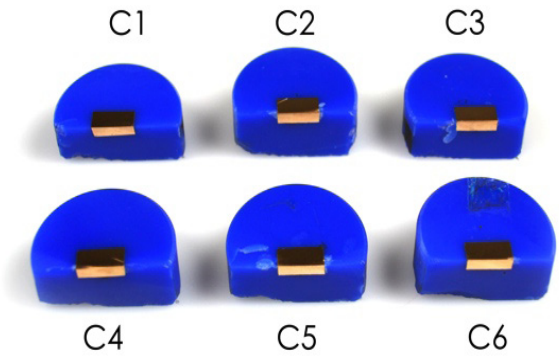

Figure 9 *C specimens, embedded for the evaluation of defects*

The experimental pieces were built without beam compensation, meaning the laser beam followed the projected geometric profile without consideration of the width of the vector produced. The absence of beam compensation led to a slightly larger part than the CAD model. This effect could be advantageous because it is possible to get better compliance with the projected dimensions after the removal of metal due to finishing. The quality level of the bricks was evaluated for roughness on the faces not subjected to grinding and for inner porosity on the surface subjected to metal removal.

Many variables were considered for evaluating the alloys, namely:

- Chemical composition of alloy particles
- Supports structure and distribution
- Slope angle of the walls of the pieces contacting the supports

Chemical composition of the classic Au-Ag-Cu alloy for SLM was modified with the addition of semiconductor elements with high intrinsic electrical resistivity such as germanium and silicon. The concentration of these addition elements must be relatively low (some thousands of parts per million) to avoid excessive deterioration of the properties required for a jewelry alloy. However, the high electrical resistivity of these additions (Table 3) appears to allow an important laser radiation absorption increase.

Table 3 *Electrical resistivity and thermal conductivity of the principal elements used for jewelry production*

Chemical elements	Electrical resistivity (mΩ·m)	Thermal conductivity (W/mK)
Silver	0.01587	429
Copper	0.01678	401
Gold	0.02214	318
Palladium	0.10540	71.8
Platinum	0.10500	71.6
Nickel	0.06849	90.7
Cobalt	0.06240	100
Zinc	0.05900	116
Tin	0.11500	66.8
Indium	0.08370	81.8
Gallium	0.27000	40.6
Germanium	5.7×10^{5}	60.2
Silicon	6.4×10^{8}	149
Ruthenium	0.071	117
Rhodium	0.0433	150
Iridium	0.0471	147
Carbon (diamond)	10^{20}	1600
Carbon (graphite)	$370 – 3\times10^{5}$	25 - 470
Carbon (amorphous)	6.5×10^{4}	10
Boron	6.5×10^{8}	27.4
Phosphorus (white)	10^{17}	0.236
Phosphorus (black)	10^{17}	12.1
Beryllium	0.03699	200
Manganese	1.43000	7.82

In general, higher electrical resistivity means lower thermal conductivity of the alloy powder, leading to a better conservation of laser energy in the target zone and correspondingly more effective localized melting. In principle, we should then have a concentration of laser energy in a smaller heat zone, resulting in an increase of local temperature and of the wetting ability (reduced surface tension) of the molten alloy. This phenomenon is more pronounced in gold alloys with semiconductor elements added, where a lower contact angle of the melt and reduced surface roughness of the pieces produced were observed, even though the melting temperature is the same for both alloys. The smoother surface is the result of shape retention of a low contact angle melt pool because solidification is very rapid.

In the case of a 950‰ platinum alloy, platinum is by far the most important component; therefore, thermal conductivity of the alloy is very near to the value of pure platinum (71W/mK). For a classic 750‰ gold alloy, we have the higher thermal conductivity of pure gold and its alloying partners (Cu, Ag), so the resulting thermal conductivity is about five times higher than that of platinum. However, the addition of low concentrations of semiconductor elements (Ge, Si, B) fundamentally improves gold alloys used for SLM, resulting in reduced surface roughness and inner porosity values. The values obtained are similar to the best pieces of the past research work.

The physical-chemical mechanism of the effect alloy composition has on absorption of laser light still waits for a thorough explanation, but it probably concerns both reflection of laser radiation and conduction of thermal energy. If we hypothesize that, initially, optical interaction could be the most important effect, the presence of extremely thin layers of oxidized compounds (GeO, SiO) or of nanoroughness could reduce reflection of laser radiation and thereby increase absorption by the alloy particles. Subsequently, the thermal energy may stay more or less confined in the target zone of the laser beam, depending on the thermal conductivity of the alloy, causing a more or less effective local melting of the powder.

In the preceding research, gallium was added to 18K gold.[1] In this work, an addition of germanium was used to investigate the changes caused by this element on surface roughness and interior porosity. A similar comparison was carried out with a 950‰ platinum alloy to evaluate the effect of a lower thermal conductivity (i.e., higher electrical resistivity) element, when it is by far the major component of the alloy.

We compared the effect of doping a classical alloy with the behavior of an alloy with a high content of a more electrically resistive metal. We planned a set of experiments with the software Materialise (Magics 17.02) for the creation and application of the support system for the pieces. This study considered two main types of support structures to evaluate their behavior.

Two different networks of support elements formed the first support type, called a block, where both spacing (1.00 and 1.50mm) and contact point area with the base of the piece were modified (Figures 10 and 11). A block-type structure is made up of three foundation levels, with an array of pilasters making the first and third. The first level is a square grid of large vertical posts that are horizontally connected to the build platform at the bottom and a seal plate at the top to form a very strong structure. The second level is a triangulated truss giving the structure great rigidity against lateral forces, and the third level is an array of smaller columns that the piece is built on. This arrangement allows the support connection point with the piece to be as small as possible for easy detachment and finishing. It was these pilasters that were modified as mentioned.

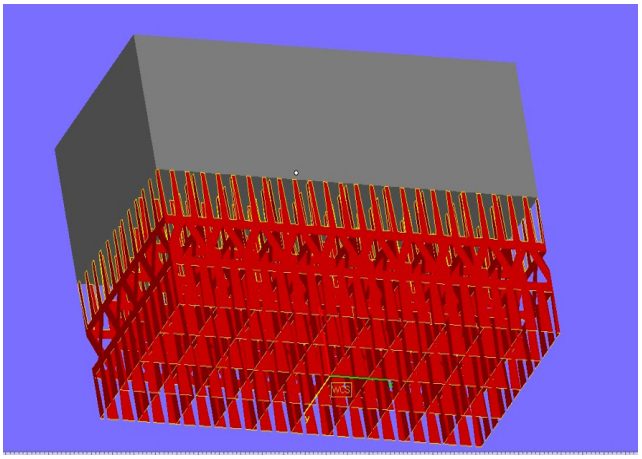

Figure 10 *Block support with 0.10mm contact area with the piece*

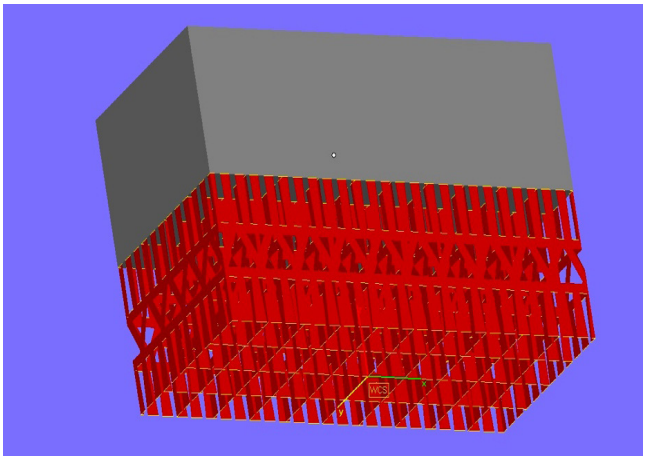

Figure 11 *Block support with 0.2mm contact area with the piece*

The second type, called volume supports, is a pillar array having square or rectangular cross sections and is attached to the build platform at the bottom and directly to the piece at the top. The spacing between the supports was set at 1.00 and 1.50mm, as seen in Figures 12 and 13. The nominal contact area of each pillar with the piece was the same for both the 1.00 and 1.50mm spacing, about 0.69mm^2.

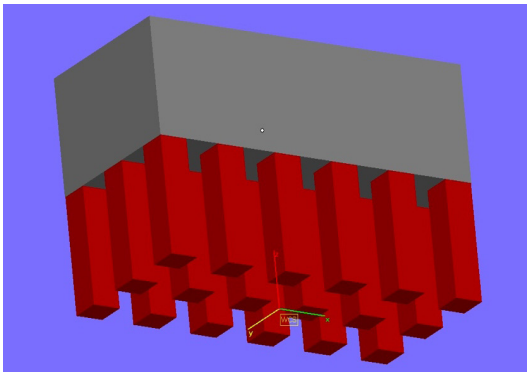

Figure 12 *Volume support with 1.00mm spacing and square contact area of 0.69mm^2*

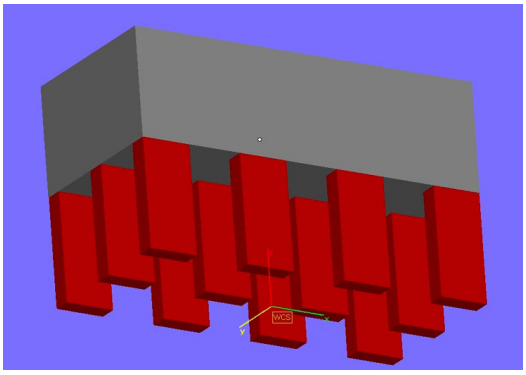

Figure 13 *Volume support with 1.50mm spacing and rectangular contact area of 0.69mm^2*

All described support configurations were applied with three different slope angles of the pieces with respect to the horizontal build platform, i.e., 0°, 20° and 40° (Figures 14, 15 and 16). A design of experiment (DOE) approach was taken to subdivide the builds according to support type, support spacing, piece slope angle and alloy (Table 4).

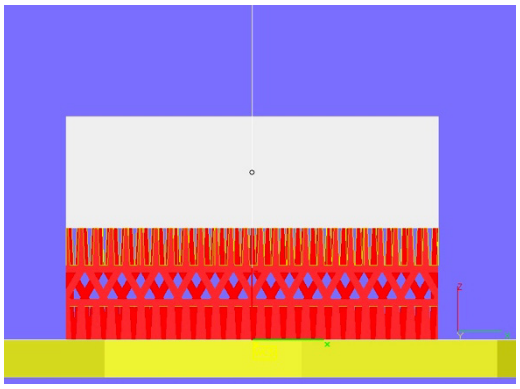

Figure 14 *Piece with 0° slope angle*

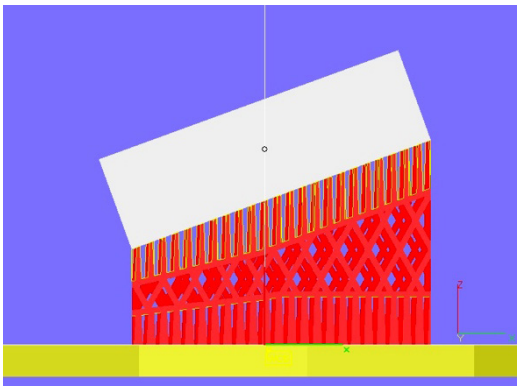

Figure 15 *Piece with 20° slope angle*

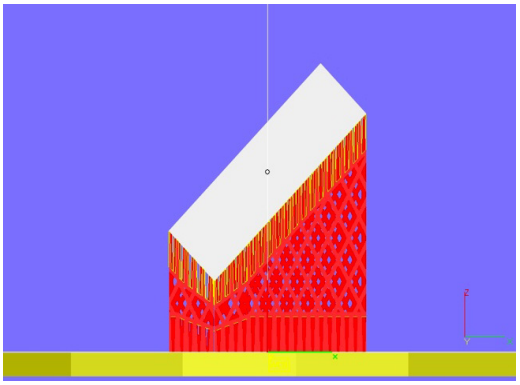

Figure 16 *Piece with 40° slope angle*

The dimensional deviation from the designed values (10.00, 4.50 and 3.00mm) was evaluated with a centesimal digital caliper (Mitutoyo) and was always positive, i.e., the built pieces were always larger than the nominal values. This phenomenon is likely attributable to the lack of beam compensation in the building process, i.e., to the cumulative effect of the side expansion of the liquid alloy (100mm), the width of the laser beam (10mm) and the surface roughness caused by the adhesion of partially melted particles.

Table 4 *Parameters and characteristic outline for the germanium-doped gold alloy and for the platinum alloy*

Support type	Support spacing (mm)	Slope angle (°)	Top length (mm)	Test identification
Block	1.00	0	0.25	A1
			0.10	A2
		20	0.25	A3
			0.10	A4
		40	0.25	A5
			0.10	A6
	1.50	0	0.25	B1
			0.10	B2
		20	0.25	B3
			0.10	B4
		40	0.25	B5
			0.10	B6
Volume	1.00	0	0.83	C1
		20	0.83	C2
		40	0.83	C3
	1.50	0	1.38	C4
		20	1.38	C5
		40	1.38	C6

RESULTS AND DISCUSSION

Our experiments were carried out with a gold alloy doped with a small amount of a semiconductor element and with a 950‰ Pt alloy having appreciably lower thermal conductivity than the gold alloy. We observed a significant difference in behavior with the same laser parameters. This behavior confirmed the important effect of an alloy with a lower thermal conductivity when compared to an alloy modified with a small addition of semiconductor elements. The S4 laser power level (62.5 watts) and scanning speeds (Table 2) were found to be insufficient for the gold alloy (Figure 17). The same power was very satisfactory for melting the platinum alloy, where the larger width and better smoothness of the vectors are a proof, as seen in Figure 18. To obtain a similar density to the platinum alloy, the laser power level required an increase of 17.5 watts for the Au 750‰ alloy, using the same scanning speed.

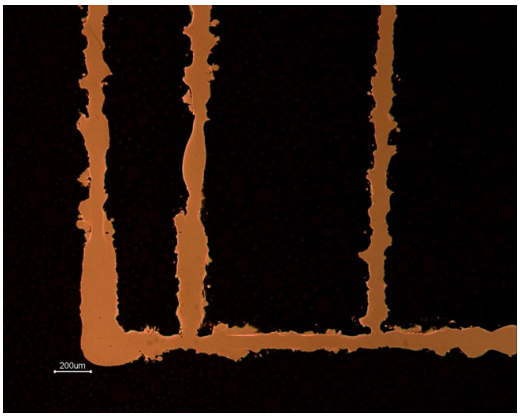

Figure 17 *Gold vectors with 62.5 watts laser power and 0.33m/s scanning speed*

Figure 18 *Platinum vectors with 62.5 watts laser power and 0.33m/s scanning speed*

As the slope angle increased, longer supports were required under the high end of the piece and therefore, the support weight increased proportionally. Volume support involves a larger weight percentage because of the greater thickness of the support. Moreover, for the same reason, detachment of the piece from the support by thermal contraction is less frequent with volume support. The problem of support detachment from the piece is usually present with the lower slope angles (0°, 20°) and decreases with an increase in the slope angle. This is because the cross section of the support attachment point is divided into more layers. The laser melts a smaller area with each scan and the amount of thermal shrinkage is proportional to the size of the melted pool.

Next, the research work was focused on the supports with the aim of finding what influence the support structure type has on the quality level of the pieces and metal loss caused by finishing. In this set of experiments, the slope angle was kept constant at 40°; only the structure of the supports was changed (Figure 19). Some macroscopic defects, such as support fracture or crumbling of partially melted particles, can be attributed to the structure of the support system. The fact that these defects are not random was demonstrated by repeating the same build experiment many times.

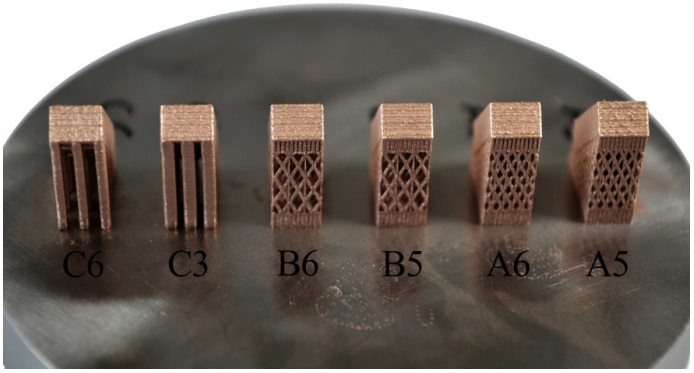

Figure 19 *The build platform of gold alloy pieces with 40° slope angle and different structure of the supports*

Pliers with plastic-coated jaws were used to manually detach the supports from the pieces to evaluate their strength and the size of residue left at the breaking point. The block support pieces, in both gold and platinum, built with the same slope and support spacing, showed less support residue when built with a 0.10mm attachment point than the specimens built with 0.25mm point. For the volume-type supports, the pieces built with the same slope angle showed less support residue when 1.5mm support spacing was used rather than 1.0mm spacing. A comparison among the different specimens showed that with an increasing slope angle, the amount of residues left on the piece tended to decrease, providing a better surface finish with markedly lower roughness (Figure 20).

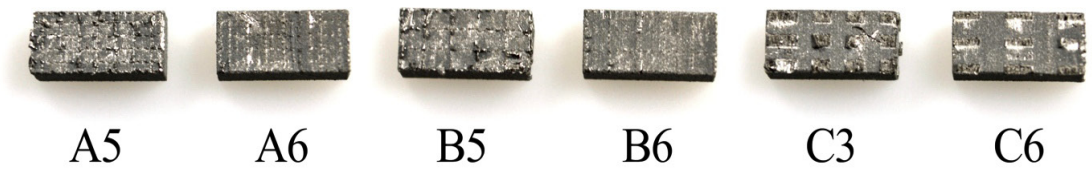

Figure 20 *Six platinum specimens (Table 4), showing the residue after removal of the supports*

After removing the supports, we determined the dimensional variation of the raw specimens compared with the software design values and the weight percentage (%w) of the supports compared with the total mass (Table 5). On average, the built length of both volume- and block-type supports is 0.35mm greater than the design value. This length increment (ΔL) tends to increase because of the presence of supports on a side face of the specimens (Figure 16). In all cases, the built width shows the same increase (ΔW) of 0.20mm because of the absence of supports and the unidirectional slope of the specimens. The height (i.e., the thickness) of the specimens requires a different consideration. Initially, because of the manual detachment of the pieces, the increase is significant and very variable, in a range (ΔH) that could go from 0.20 to 0.90mm.

To carry out quality evaluations, the specimens were embedded in epoxy resin. For the first evaluation, the specimens were taken in steps to a precise thickness of 3.00mm using automated grinding and measuring the progress between each step. Once the specimens reached 3.00mm, the surface was scrutinized and compared to evaluate the general amount of defects (Figure 21). A second and more detailed evaluation of each specimen was carried out after removing another 0.20mm to make it 2.80mm thick (Figure 22). Then the specimens were evaluated for internal porosity using automatic equipment. The values are reported in Table 5.

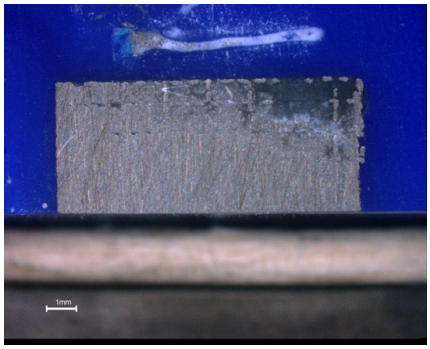

Figure 21 *A5 specimen ground to a precise thickness of 3.00mm for the first evaluation*

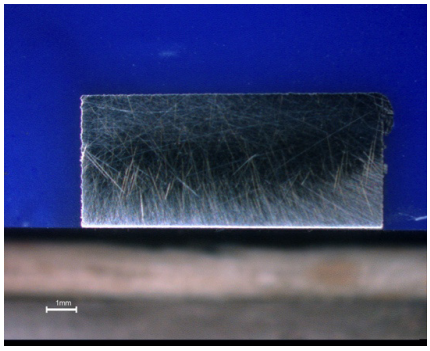

Figure 21 *A5 specimen ground to a precise thickness of 2.80mm for the second evaluation*

Table 5 *Test parameters, dimensional values and porosity data for the germanium-doped gold alloy*

Support type	Support spacing (mm)	Slope angle (°)	Top length (mm)	Test identification	%w*	DL (mm)	DW (mm)	DH (mm)	% porosity
Block	1.00	0	0.25	A1	29	+0.30	+0.20	+0.70	0.14
			0.10	A2	16	+0.30	+0.20	+0.65	0.21
		20	0.25	A3	28	+0.30	+0.20	+0.50	0.10
			0.10	A4	30	+0.30	+0.20	+0.20	0.05
		40	0.25	A5	57	+0.40	+0.20	+0.45	0.06
			0.10	A6	44	+0.40	+0.20	+0.45	0.09
	1.50	0	0.25	B1	17	+0.30	+0.20	+0.90	0.63
			0.10	B2	13	+0.30	+0.20	+0.80	0.58
		20	0.25	B3	21	+0.30	+0.20	+0.50	0.10
			0.10	B4	26	+0.30	+0.20	+0.30	0.10
		40	0.25	B5	31	+0.60	+0.20	+0.50	0.03
			0.10	B6	22	+0.50	+0.20	+0.40	0.23
Volume	1.00	0	0.83	C1	34	+0.30	+0.20	+0.75	0.10
		20	0.83	C2	49	+0.30	+0.20	+0.70	0.12
		40	0.83	C3	89	+0.40	+0.20	+0.75	0.13
	1.50	0	1.38	C4	24	+0.30	+0.20	+0.90	0.05
		20	1.38	C5	36	+0.30	+0.20	+0.75	0.06
		40	1.38	C6	59	+0.30	+0.20	+0.50	0.04

* Weight percentage of the supports compared to the total mass

The high porosity level observed in specimen B1 probably resulted from a bad fracture in the supports, causing a serious alteration of the building process that extended into the interior of the piece. The fracture began about halfway up the support structure where the support spacing is wider than above or below that point and was due to thermal contraction of the alloy (Figure 23).

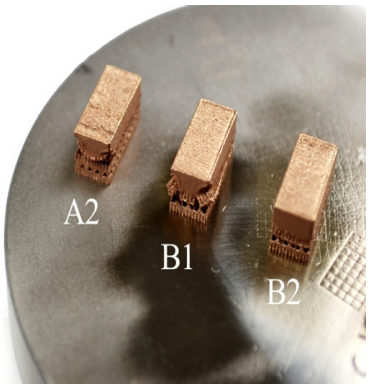

Figure 23 *B1 specimen with fractured supports*

We observed decreasing internal porosity when the slope angle of specimen walls increased in the block-supported pieces. This is because, with increased slope angle, the surface area between the solidified alloy and the solidifying alloy was increased. For the same reason, the internal porosity also decreased when the spacing between block supports decreased; this is because the solidified supports provided increased surface area. Internal porosity was less affected by the slope angle of specimen walls for volume-supported pieces, and the average porosity was lower compared to block-supported pieces. However, the influence of volume-support spacing on porosity is opposite that of block-supported pieces; porosity appears to decrease as volume-support spacing increases. This probably happens because the gold alloy has higher thermal conductivity, so with reduced support cross section, less heat is lost and laser energy is used more efficiently.

While the dimensional variations and internal porosity of the 950‰ platinum alloy follow the same trends of the gold alloy, the values were lower (Table 6). The Pt supports represent a lower weight percentage in comparison to the gold alloy. This can be attributed to the higher melting point, which allowed thinner vectors to be built and consequently lighter supports. Better definition of the Pt vectors results in better dimensional compliance and, therefore, lower variability than in the gold alloy.

Table 6 Parameters and typical data for the 950‰ platinum alloy

Support type	Support spacing (mm)	Slope angle (°)	Top length (mm)	Test identification	%w*	DL (mm)	DW (mm)	DH (mm)	% porosity
Block	1.00	0	0.25	A1	13.5	+0.15	+0.09	+1.00	0.01
			0.10	A2	15.0	+0.15	+0.12	+0.41	0.05
		20	0.25	A3	21.5	+0.18	+0.08	+0.40	0.02
			0.10	A4	24.0	+0.38	+0.11	+0.22	0.02
		40	0.25	A5	26.0	+0.58	+0.12	+0.52	0.02
			0.10	A6	27.3	+0.30	+0.12	+0.32	0.06
	1.50	0	0.25	B1	11.2	+0.18	+0.12	+0.71	0.05
			0.10	B2	10.2	+0.18	+0.11	+0.65	0.03
		20	0.25	B3	17.1	+0.18	+0.14	+0.34	0.01
			0.10	B4	16.1	+0.20	+0.12	+0.28	0.03
		40	0.25	B5	18.8	+0.48	+0.15	+0.50	0.03
			0.10	B6	18.5	+0.40	+0.12	+0.33	0.01
Volume	1.00	0	0.83	C1	22.5	+0.18	+0.12	+0.50	0.02
		20	0.83	C2	32.3	+0.15	+0.12	+0.55	0.02
		40	0.83	C3	41.7	+0.52	+0.12	+0.58	0.05
	1.50	0	1.38	C4	17.3	+0.15	+0.11	+0.76	0.03
		20	1.38	C5	27.0	+0.20	+0.13	+0.57	0.01
		40	1.38	C6	32.6	+0.38	+0.12	+0.40	0.01

* Weight percentage of the supports compared to the total mass

The markedly lower internal porosity in the platinum alloy can be explained by its low thermal conductivity. This results in more efficient building of the vectors due to low diffusion of laser radiation energy during melting. To avoid interference from local macroscopic defects that were not related to the melting process in specimens A4, B4 and C2 (Table 6), the evaluation of internal porosity was carried out in the zones with the best quality microstructure (Figures 24 and 25).

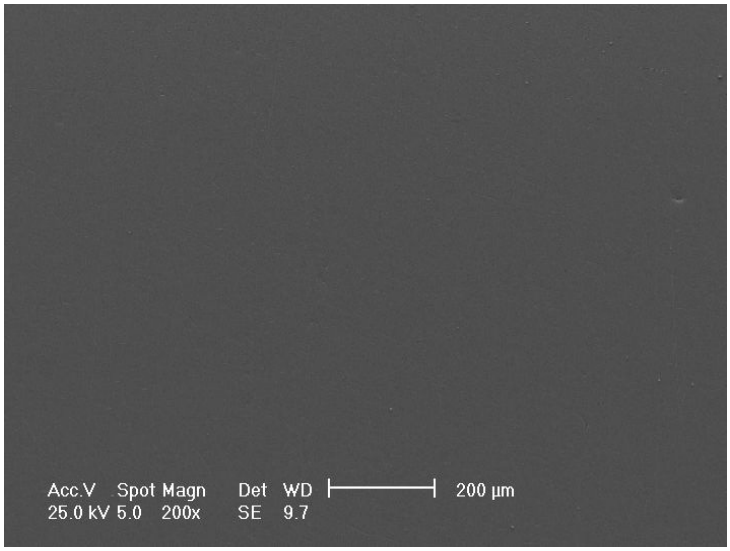

Figure 24 *SEM cross section, specimen A4 (platinum)*

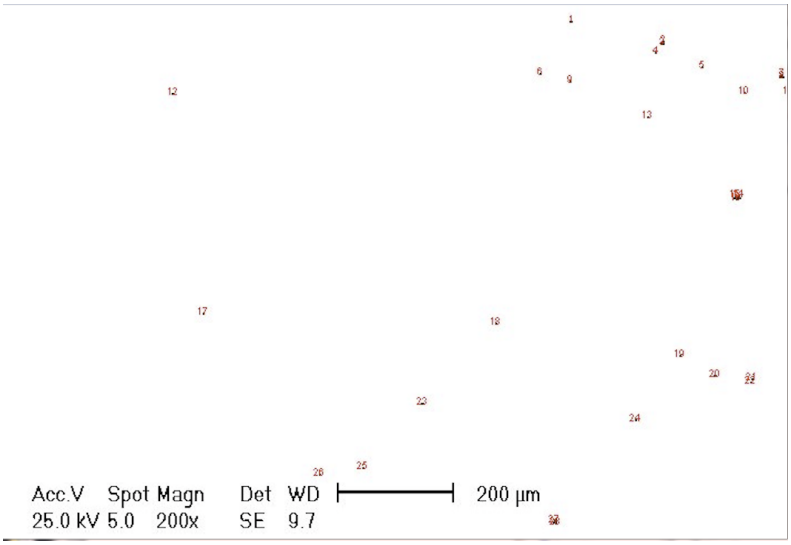

Figure 25 *Example of digital porosity evaluation*

In previous work, the formation of swelling on low-slope angle walls was observed as a possible problem for gold alloys. This problem can be partially ascribed to the presence of gallium in the alloy.[2] The present work has demonstrated that it is possible to improve SLM of a classic 18K alloy through the addition of small quantities of semiconductor elements such as silicon, germanium and boron. On surfaces parallel to the build platform, the germanium-doped gold alloy obtained a total roughness R_t = 55µm. That is about 30% lower than the figure obtained with the same alloy without the germanium addition (Figures 26 and 27). However, in a specimen built with alloy 1, the roughness was further reduced to about R_t = 40µm by increasing the laser power to 80W (Figure 28). This improvement resulted in smoother surfaces and consequently reduced time and weight loss in finishing. The difference in quality between the germanium-doped gold specimens and low thermal-conductivity platinum alloy specimens was observed. Total roughness of the platinum alloy was R_t = 78µm. This value is not only influenced by lower laser power (62.5W), but also because the alloy has higher surface tension in the molten state compared to the gold alloy.

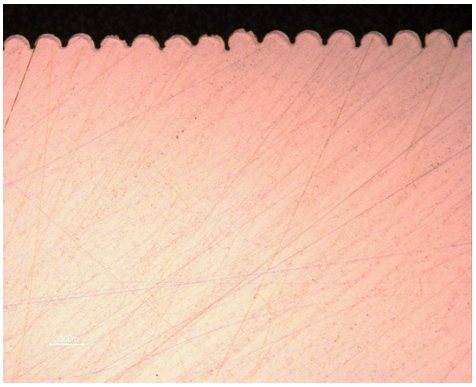

Figure 26 *Germanium-free gold alloy, 72.5W laser power*

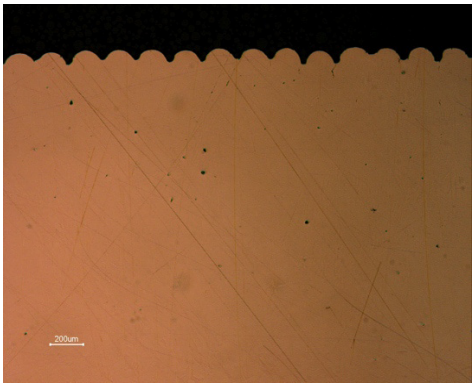

Figure 27 *Gold alloy with germanium addition, 72.5W laser power*

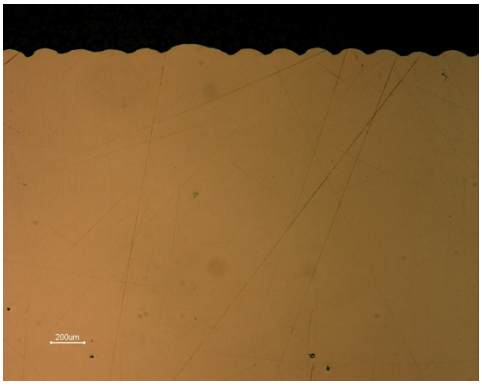

Figure 28 *Gold alloy with germanium addition, 80W laser power*

Figure 29 illustrates the beneficial effect of a shorter distance between support elements. A bridge effect always provides a route for heat transmission from the molten metal into a sufficient amount of solid alloy to weld the molten particles in the subsequent scans. We believe that this mechanism is most efficient when the space (*g*) between the points is narrower than the width (*w*) of the molten vector and the spacing between the vectors (*d*) (*hatch distance*) is smaller than the width of the molten vector (*w*). These parameters provide a good connection between the vectors, a thinner (*h* = 150µm) spongy zone in the piece and minimize the support residue where it is detached from the piece.

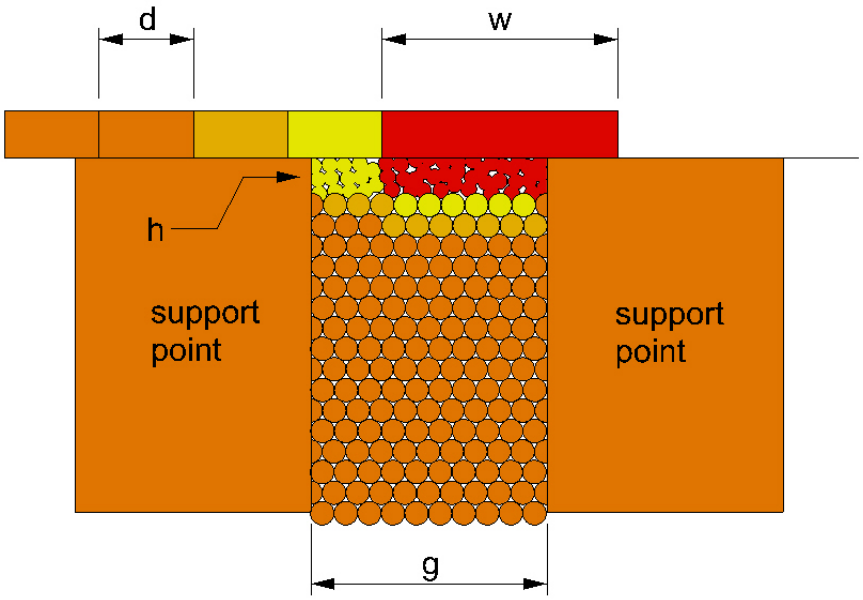

Figure 29 *Heat dissipation mechanism with bridge effect*

Figure 30 illustrates the case of volume supports; the distance (*g*) between the supports is wider than the width of the molten vector (*w*). Therefore, the thickness (*h*) of the spongy zone is greater (450µm). Also, the height of the raw specimen is notably larger than the design value (Table 6). This is because the mechanism of joining and heat transmission is less efficient, and the bridge effect has less influence, so the laser energy reaches a deeper zone and is less effective in melting the alloy. Moreover, the greater thickness of the volume supports causes a larger residue of metal to be left on the piece after it is detached. This phenomenon also takes place with the block supports when the attachment points are wider (0.25mm).

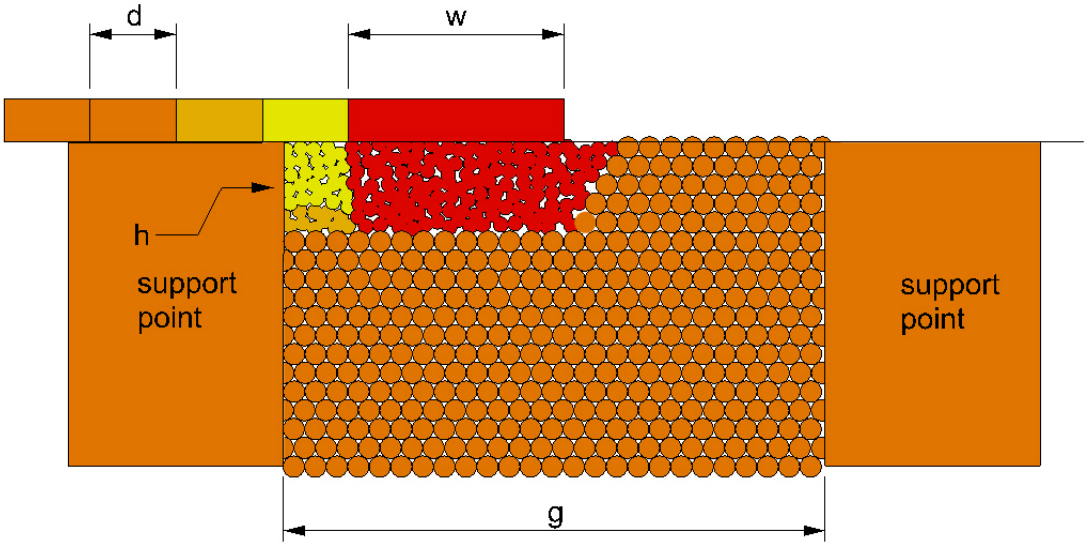

Figure 30 *Heat dissipation mechanism without bridge effect*

The experiments confirmed that building with an angle of 0°, the block supports provided a sponge zone of around 100 microns (Figures 31 and 32). Dimensional compliance with the software parameters for the support system was evaluated using SEM. For the platinum alloy built at 0° slope angle, the design size for block supports was 0.25mm and the actual as-built size was about 0.32mm on average, as seen in Figure 31. The connection points between the piece and the supports were set at 0.10mm in the Magics software, but the actual as-built dimension was 0.19mm, as seen in Figure 32.

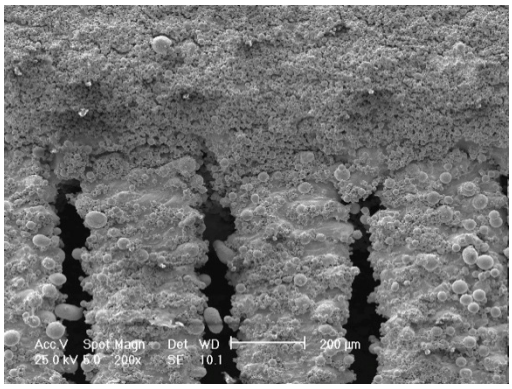

Figure 31 *A1 supports made of platinum, slope angle 0°*

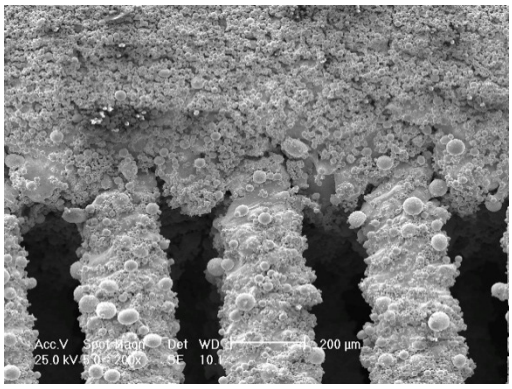

Figure 32 *A2 supports made of platinum, slope angle 0°*

For high-angle builds, the sponge zone is further reduced due to the presence of a large volume of solid alloy under the molten vectors (Figures 33 and 34).

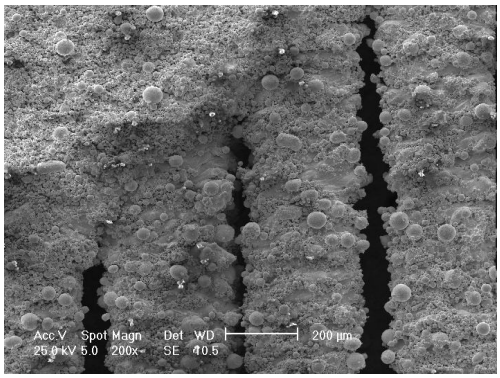

Figure 33 *A5 supports made of platinum, slope angle 40°*

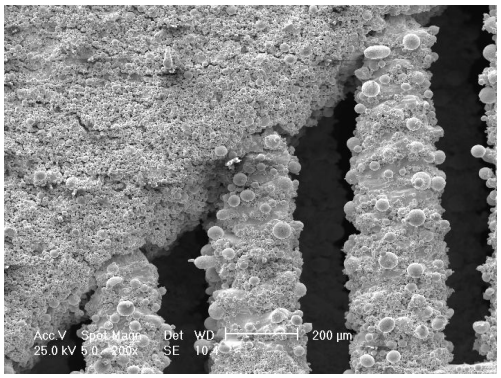

Figure 34 *A6 supports made of platinum, slope angle 40°*

The volume-support experiments built at 0° slope angle confirmed that the sponge zone is nearly twice that of the block-support specimens (Figures 35 and 36).

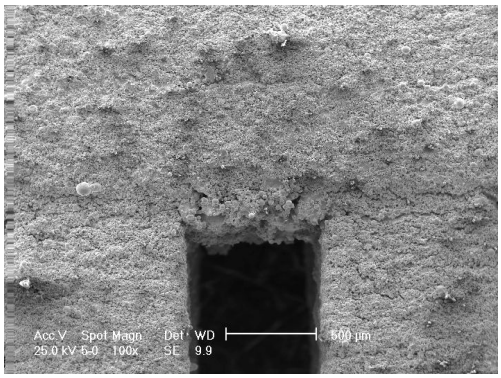

Figure 35 *C1 supports made of platinum, slope angle 0°*

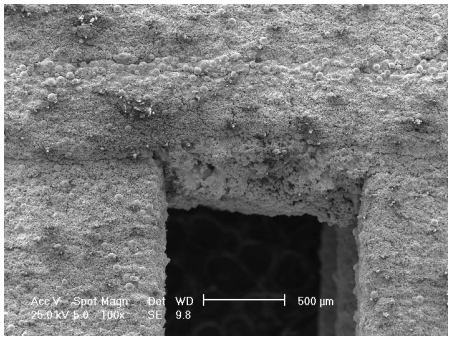

Figure 36 *C4 supports made of platinum, slope angle 0°*

For high-angle builds with volume supports, the large amount of solid alloy under the molten vectors greatly reduced the sponge zone. It appears that, in this case, the slope angle has more influence on the sponge zone than the support spacing, as seen in Figure 37 (1.00mm spacing) and Figure 38 (1.50mm spacing).

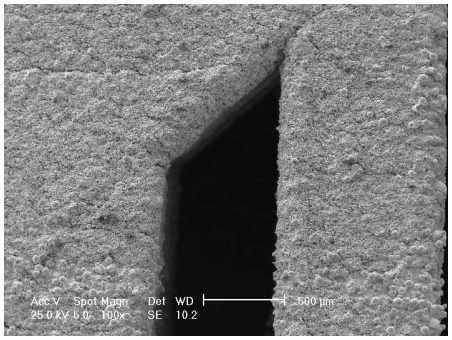

Figure 37 *C3 supports made of platinum, slope angle 40°*

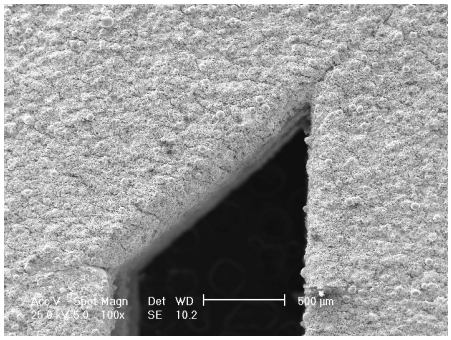

Figure 38 *C6 supports made of platinum, slope angle 40°*

Some specimens made of gold alloy powder or platinum alloy powder showed macroscopic defects. The defects in the gold alloy were present only in the A2, A4 and B4 specimens. For these specimens, the slope angle was 0° and 20°, with 0.10mm attachment points. The problem probably originates from a weak bond between the specimen and the support system, so that the thermal contraction stress caused a hot-tear fracture. However, this defect did not appear in the specimens with a 40° slope angle because the section affected by laser melting in each build layer is smaller and, consequently, there is less overall thermal contraction. More precisely, in the A2 specimen microcracks were observed, while in the A4 specimen there is a deformation of an edge caused by fracture at the supports during the building process (Figures 39 and 40).

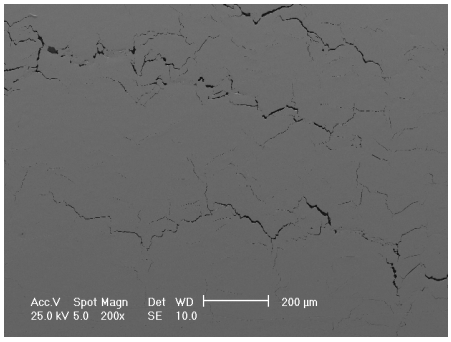

Figure 39 *A2 specimen, gold alloy, microcracks in transverse surface*

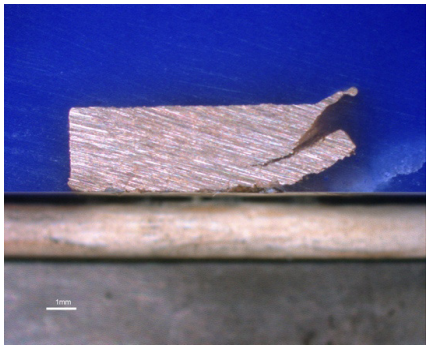

Figure 40 *A4 specimen, gold alloy, fracture in longitudinal surface*

For the platinum alloy specimens, macroscopic defects were observed only in A4, B4 and C5 specimens. All of these specimens were built with a slope angle of 20°. The A4 and B4 specimens had block supports with an attachment point width of 0.10mm. The defect in the C5 specimen is located in the zone between the volume supports spaced at 1.5mm. It is possibly caused in the building process by a discontinuity of the edge on pieces built at this slope angle. When building in the zone between widely spaced supports, heat transfer to the supports becomes poor. As the laser scan travels away from the heat sink effect of the support, a thin gap is formed between the molten vector and adjacent powder layer because of the very thin, solid cross section under the molten vector. The molten pool tends to be overheated and thus the surface tension phenomenon causes the metal to draw back (Figure 41).

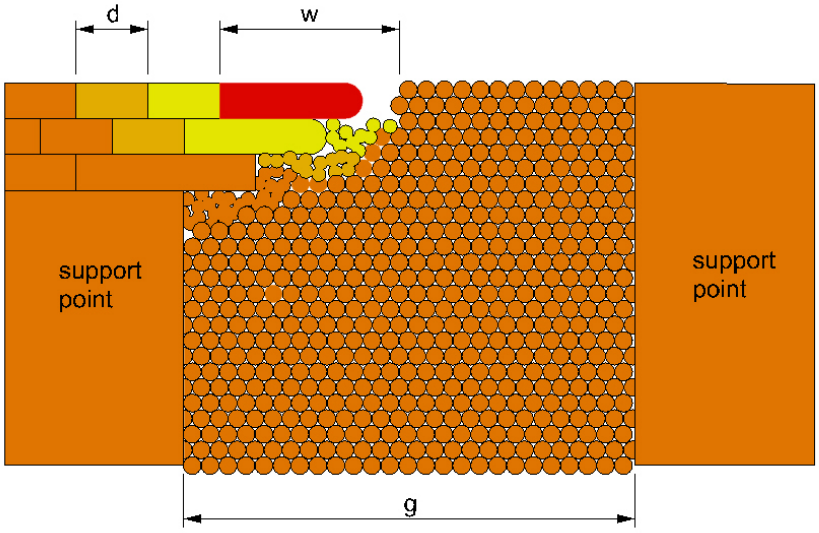

Figure 41 *Mechanism of collapsing of the sloping walls*

The subsequent wiper passes can refill this gap with new powder, but the next laser scans are focus at the next higher level, so insufficient energy is delivered to melt the lose particles in the previous layer where the gap refilled. This creates the possibility of a collapse of the bridge midway between the supports. The depth of the defect in C5 specimen is about 550µm (Figures 42, 43 and 44).

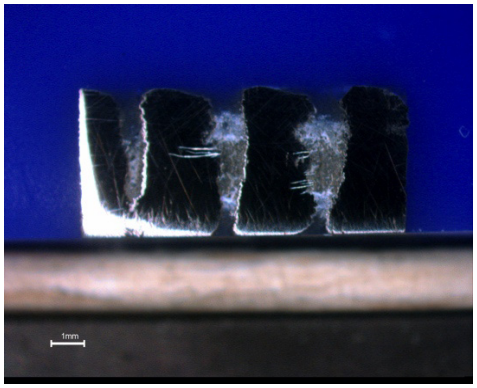

Figure 42 *Raw C5 specimen made of platinum*

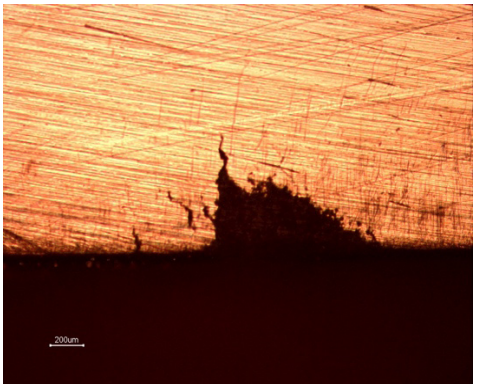

Figure 43 *Longitudinal section of C5 platinum specimen*

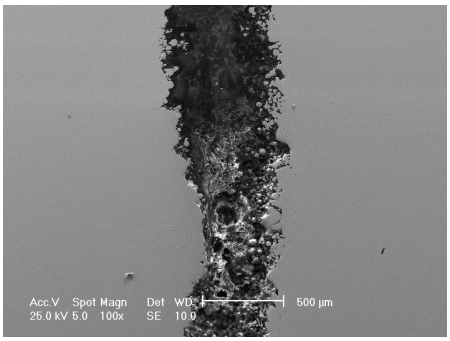

Figure 44 *SEM micrograph of the surface of the C5 platinum specimen*

Lastly, after the specimens with a 0° slope angle were ground to a thickness of 2.80mm, other less frequent defect types were observed. These defects could be classified as deep surface roughness that can be repaired with slightly more extensive finishing. This kind of roughness originated in zones where melting was particularly difficult and the formation of a sound alloy layer was prevented (Figures 45 and 46).

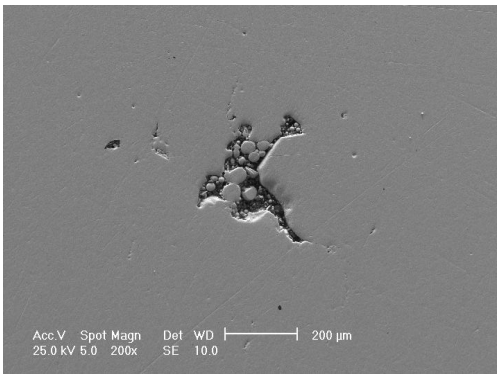

Figure 45 *A1 specimen after lapping, 200X*

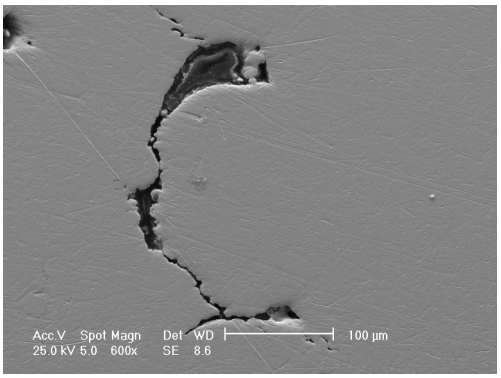

Figure 46 *A2 specimen after lapping, 200X*

CONCLUSIONS

In this work, we demonstrated the possibility of increasing the absorption of laser radiation with a reduction of reflected and dispersed energy to obtain a more efficient melting of alloy particles. This objective was achieved through two ways:

1. The use of a precious alloy with a thermal conductivity significantly lower than usual gold alloys, e.g., a high fineness (950‰) platinum alloy
2. With the addition of a small concentration of semiconductor elements (Si, Ge) that, thanks to their higher electrical resistivity, can reduce the thermal conductivity of the gold alloy and improve the SLM behavior

The presence of semiconductor elements, with a concentration of a few thousands of parts per million, produced a 30% reduction in surface roughness of the specimens and a reduction of the amount of particles ejected by the laser beam, which is a cause of the formation of bulges. Moreover, a good quality microstructure was obtained with a low 0.03% porosity near the support system, which is the most problematic area. This opened the way to a new approach for SLM that is not only based on the selection of laser parameters but also on the ability of the alloy to more efficiently transform the laser radiation into fusion heat in the alloy particles. The addition of a low concentration of a semiconductor element greatly improved the suitability of a gold alloy for SLM in terms of less surface roughness and process stability. More generally, it was shown that an alloy naturally having low thermal conductivity, such as 950‰ platinum, produced lower porosity levels than the higher conductivity gold alloy, even when the gold is doped.

To study the role of the support system, we varied its shape, spacing and connection slope. In general, we found that thinner supports are more easily detached and are advisable for high-slope walls, while more massive supports are advisable for more horizontal walls. These parameters reduce defects at the support connection point due to thermal contraction stresses. Finally, the research shows that surface quality can be optimized and processing loss reduced when the correct selection between thin and massive supports is made.

REFERENCES

1. D. Zito et al., “Optimization of the Main Selective Laser Melting Technology Parameters in the Production of Gold Jewelry,” *The Santa Fe Symposium on Jewelry Manufacturing Technology 2013*, ed. E. Bell and J. Haldeman (Albuquerque: Met-Chem Research, 2013): 383-402.

2. J. Kruth et al., “Binding mechanisms in selective laser sintering and selective laser melting,” *Proceedings of the Solid Freeform Fabrication Symposium* (2004): 44-59.

3. D. Zito et al., “Latest developments in Selective Laser Melting Production of Gold Jewelry,” *The Santa Fe Symposium on Jewelry Manufacturing Technology 2012*, ed. E. Bell (Albuquerque: Met-Chem Research 2012): 537-562.

4. Y. Yadroitsev et al., “Factor analysis of selective laser melting process parameters and geometrical characteristics of synthesized single tracks,” *Rapid Prototyping Journal* 18, no. 3 (2012): 201-208.

5. J.P. Kruth and S. Kumar, “Statistical Analysis of Experimental Parameters in Selective Laser Sintering,” *Advanced Engineering Materials* 7, no. 8 (August 2005): 750-755.